Journal of Alloys and Compounds 931 (2023) 167498

Contents lists available at ScienceDirect

Journal of Alloys and Compounds

journal homepage: www.elsevier.com/locate/jalcom

Research article

High strength and high ductility of Mg-10Gd-3Y alloy achieved by a novel extrusion-shearing process

Cai Chen [a,*], Dongsheng Han [a], Mingchuan Wang [a], Shun Xu [b,*], Ting Cai [a], Sen Yang [c], Fengjian Shi [d], Benoit Beausir [e], Laszlo S. Toth [e,f,**]

[a] Sino-French Engineer School, Nanjing University of Science and Technology, Xiaolingwei 200, Nanjing 210094, China
[b] National Key Laboratory of Science and Technology on Materials under Shock and Impact, School of Materials Science and Engineering, Beijing Institute of Technology, Beijing 100081, China
[c] School of Materials Science and Engineering, Nanjing University of Science and Technology, Xiaolingwei 200, Nanjing 210094, China
[d] School of Materials Science and Engineering, Jiangsu University of Science and Technology, Zhenjiang 212003, China
[e] Laboratoire d'Etude des Microstructures et de Mécanique des Matériaux (LEM3), UMR 7239, CNRS/Université de Lorraine, F-57045 Metz, France
[f] Institute of Physical Metallurgy, Metal-forming and Nanotechnology, University of Miskolc, Miskolc, Hungary

ARTICLE INFO

Article history:
Received 14 August 2022
Received in revised form 3 October 2022
Accepted 6 October 2022
Available online 8 October 2022

Keywords:
Mg-Gd-Y
Extrusion-shearing
Strength and ductility
Precipitate
Crystallographic texture

ABSTRACT

To simultaneously improve the strength and ductility of the Mg-10Gd-3Y alloy, we propose a new processing route: conventional extrusion (EX), followed by an equal channel angular pressing (ECAP) deformation, without stopping. The new process is called: extrusion-shearing (ES). By employing ES at 400 °C, the tensile yield strength of the Mg-10Gd-3Y alloy was increased to 289 MPa, together with a high ultimate tensile strength of 361 MPa, and a good tensile elongation to failure of 27.4 %, at room temperature. The underlying mechanisms for the simultaneous enhancement in strength and ductility were investigated. The extra shearing deformation by the ECAP-stage of the ES testing led to the formation of a fully recrystallized homogenous microstructure with an average grain size of 4.3 μm, with dynamic precipitation of $Mg_5(Gd,Y)$ particles at/near grain boundaries. Both macro and micro texture characterizations indicated a strong decrease in the intensity of the crystallographic texture during the ECAP part of the ES process, and a new type of texture. The multicomponent nature of the obtained texture and the microstructural modifications together with a dispersive distribution of precipitates contributed to an excellent combination of high strength and ductility of the Mg-10Gd-3Y alloy processed by ES.

1. Introduction

Mg alloys are of great interest due to their potential applications as lightweight structural materials in aerospace and automotive industries [1–3]. However, the relatively poor strength and low ductility limit their application in the industry, which triggers the research by adding rare-earth (RE) elements into Mg for the purpose of improving strength and ductility of Mg alloy, called Mg-RE alloy [4]. The effect of RE on recrystallization behavior, grain refinement mechanism, precipitate distribution and crystallographic texture in Mg-RE alloy are discussed in Refs. [2,5–7]. With the addition of Gd, the strength of Mg alloy can be enhanced by solute solution and precipitate strengthening [8,9]. Since Y is an efficient RE element for the improvement of ductility of Mg alloys [10,11], optimization of composition and microstructure to fabricate ternary Mg-Gd-Y alloy with high-performance is a hot topic during the last decade [11].

Another effective way that can improve the mechanical property of Mg is to refine the grains via the well-known Hall-Patch relationship. Hot extrusion, as a common method of thermo-mechanical treatments, has been widely used to improve the mechanical properties of Mg-Gd-Y alloy by grain refinement [12]. During extrusion process, dynamic recrystallization (DRX) of the Mg matrix and dynamic precipitation (DP) of second phases are considered as the mechanism for grain refinement [13]. However, after extrusion process, a heterogenous microstructure and precipitate distribution, as well as a high intensity of basal texture [14] is usually formed, leading to unacceptable mechanical properties for industrial application. In order to obtain a smaller grain size of the Mg matrix and dispersive distribution of precipitates, an extremely large

* Corresponding authors.
** Corresponding author at: Sino-French Engineer School, Nanjing University of Science and Technology, Xiaolingwei 200, Nanjing 210094, China.
E-mail addresses: cai.chen@njust.edu.cn (C. Chen), shunxu@bit.edu.cn (S. Xu), laszlo.toth@univ-lorraine.fr (L.S. Toth).

https://doi.org/10.1016/j.jallcom.2022.167498
0925-8388/

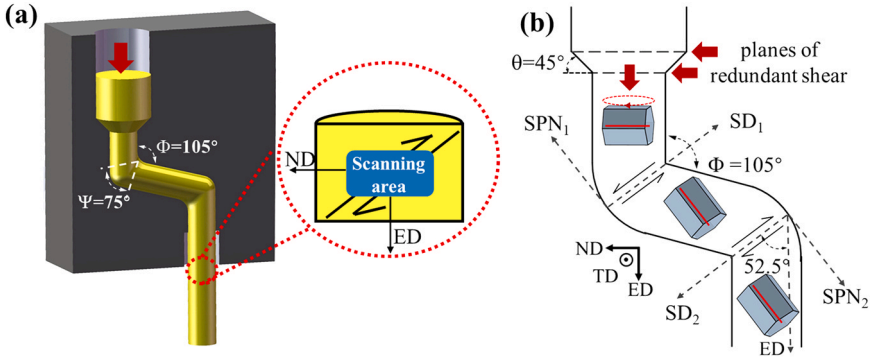

Fig. 1. Schematic illustrations of the ES process (a); Places of shear deformations and crystal rotation of the main orientation component in the ECAP part of the ES process (b).

extrusion ratio is usually needed, which is a limitation for the application of EX process in the production of Mg-Gd-Y alloy. There is also another problem that the formation of a strong basal texture during the extrusion process results in poor ductility during tensile testing at room temperature. Therefore, tuning the texture for the improvement of ductility of Mg alloys needs further investigations.

Beside the conventional extrusion (EX) process, simple shear based severe plastic deformation (SPD) is another promising candidate for improving the mechanical properties by efficient microstructure fragmentation process, which is widely used in Mg and its alloys [15–17]. The equal channel angular pressing (ECAP) process is considered as a potential technique for industrial application due to its capacity for large-scale processing. ECAP is proved to be an efficient method for enhancing the ductility of Mg alloy, without sacrificing strength [14,18,19]. A combination of hot extrusion and two ECAP passes, called ES processing, is proposed recently [20]. It is an efficient technique for further refining the microstructure of Mg-RE alloys [20–23]. In order to improve the strength of the Mg-10Gd-3Y (wt%) alloy without loss of ductility, we applied the extrusion-shearing (ES) process to modify its microstructure and texture to achieve high performance. In our experiments, the ultimate tensile strength (UTS) reached 361 MPa with a high elongation to failure (EL) of 27.4 %. The underlying mechanisms were investigated for understanding the excellent combination of high strength and ductility of the Mg-10Gd-3Y alloy. This alloy is also called as GW103 [24].

2. Materials and methods

The nominal composition of Mg-10Gd-3Y (wt%) alloy used in this work was produced via sand casting. High purity Mg (> 99.7 wt%), Mg-30Gd, and Mg-30Y (wt%) master alloys were used in an electric resistance furnace at about 760 ℃, under a mixed gas atmosphere of SF_6 and CO_2. The exact composition was determined to be Mg-10.62Gd-3.21Y by using an inductive coupled plasma spectrometer analyzer. The ingots were homogenized at 530 ℃ for 10 h, followed by quenching into warm water. All billets were preheated at 420 ℃ for 30 min and then extruded at 400 ℃, at a speed of 22 mm/s. The alloy was processed by conventional hot extrusion at 400 °C with an extrusion ratio of 4:1 (EX4), and by the ES method. Lower temperature did not permit to obtain a continuous sample. As shown in Fig. 1, the ES method includes the EX4 process followed by two ECAP passes in route C, with a die angle of Φ = 105° and rounding angle at the outer corner of Ψ = 75°. The dimensional data of the testing are listed in Table 1. The obtained strain values are expressed in von-Mises equivalent strain ($\bar{\varepsilon}$) in Eqs. (1–3). For the EX4 process, the redundant shear is also accounted for, it varies within the obtained bar linearly from the center to the surface (Eq. 2), where the position within the bar is expressed by the ζ parameter, which is 0 in the center of the sample and 1 at the surface.

$$\text{v} - \text{M strain for extrusion:} \quad \bar{\varepsilon}=ln\frac{D_0^2}{D_1^2} \tag{1}$$

$$\text{v} - \text{M strain for total redundant shear in extrusion: } \bar{\varepsilon}=\frac{2\zeta}{\sqrt{3}\ tan\theta} \tag{2}$$

$$\text{v} - \text{M strain for ECAP route C: } \bar{\varepsilon}=2\left[\frac{2cot\left(\frac{\Phi}{2}+\frac{\Psi}{2}\right)+\text{cosec}\left(\frac{\Phi}{2}+\frac{\Psi}{2}\right)}{\sqrt{3}}\right] \tag{3}$$

As can be seen in Table 1, the EX4 process itself produces a sample in which the strain varies between 1.39 and 2.54, because of the contribution of the redundant shear. By adding the ECAP route C strain, one obtains the total strain in the ES process between 2.54 and 3.69.

The microstructural observations were performed using an optical microscope (OM, Axio Vert.A1), a scanning electron microscope (SEM, Quant 250FEG) equipped with an energy dispersive X-ray spectrometer (EDS), and electron backscattered diffraction (EBSD) on the extrusion direction-normal direction (ED-ND) plane (Fig. 1). The macro-texture was revealed via X-ray diffraction (XRD, X′Pert). Dog-bone shaped samples with a gauge size of 2 mm × 3 mm× 5 mm were processed for uniaxial tensile testing, which was conducted at room temperature along the ED, at a speed of 0.5 mm/min.

3. Results

3.1. Microstructure evolution

The microstructures of the homogenized, EX4 and ES processed alloys are shown in Fig. 2. These 3D OM based results reveal that all microstructures are mainly composed of α-Mg matrix and small eutectic phases. The EX4 processed sample shows a significant bimodal structure with the combination of elongated large grains surrounded by small equiaxed grains, which is the typical microstructure of extruded Mg-Gd-Y alloy with a small extrusion ratio [25]. After the addition of two ECAP- shearing processes by ES, the microstructure is refined into homogeneous small equiaxed grains with a dispersive distribution of precipitated particles. The latter are located at/near the grain boundaries as illustrated in Fig. 3f. The grain size in the ES processed sample was dramatically smaller compared to the EX4, with homogenous microstructure.

The distribution of precipitates was investigated by SEM and EDS in Fig. 3. The precipitations in EX4 are positioned mainly along the extrusion direction with a larger average size as shown in Fig. 3a-b, however, after the ES process, the precipitation distribution is more homogenous with smaller average size as shown in Fig. 3d-e. The size distributions of the cuboid shaped particles were quite similar

Table 1
Testing dimensional data and related strain values.

Test	sample initial diameter	sample final diameter	extrusion die angle, θ	ECAP die main angle, Φ	ECAP die rounding angle, Ψ	extrusion strain	Total redundant shear	von Mises strain
EX4	20 mm	10 mm	45°	–	–	1.39	0.0 – 2.0	1.39 – 2.54
ECAP	10 mm	10 mm	–	105°	75°	1.15	–	1.15
ES	20 mm	10 mm						2.54 – 3.69

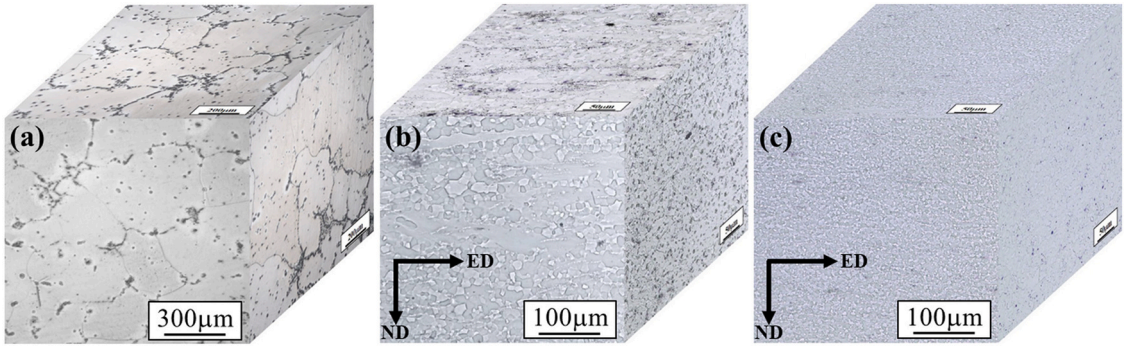

Fig. 2. Microstructure evolution in 3D of (a) homogenized; (b) EX4; (c) ES processed Mg-10Gd-3Y alloy.

between the EX4 and ES processed samples, see the histogram in Fig. 3c. Three types of precipitates were found in both processed samples: irregular precipitates (green arrows), cuboid precipitates (yellow arrows), and granular precipitates with size d < 1 μm (white arrows). The EDS results confirmed that the cuboid particles were the well-known stable $Mg_5(Gd,Y)$ β phases due to dynamic precipitation, which is extensively studied in magnesium alloys [26,27]. These cuboid particles do not contribute much to the strength of the material, due to their low volume fraction [20].

Fig. 4 shows the EBSD orientation maps in inverse pole figure (IPF) form in the ED-ND section, where the ED direction was projected. The EBSD data were analyzed using the ATEX software [28]. The low-angle grain boundaries (LAGBs; $2° \le \theta \le 15°$) and the high-angle grain boundaries (HAGBs; $\theta > 15°$) were labelled by white and red lines, respectively. 5° was considered as a minimum disorientation angle for defining a grain. The average grain sizes in the EX4 and ES processed samples were about 13.3 μm, and 4.3 μm, respectively, obtained from the average values of three maps. The grain size distribution for the ES sample could be well fitted by a Gaussian distribution function (Fig. 4e). The neighbor-to-neighbor grain disorientation distributions are shown in Figs. 4c and 4f. The proportions of the HAGBs were very high for both processes: 97.44 % and 98.83 %.

3.2. Mechanical properties

Fig. 5a displays the tensile stress-strain curves of the initial homogenized, the EX4, and ES processed samples. The tensile yield strength (YS), UTS and tensile EL are summarized in Table 2. It can be seen that both the ES and EX processes could effectively enhance the strength and ductility of the materials. Especially, the ES processed sample showed significant improvement in strength with a YS of 289 MPa and UTS of 361 MPa (engineering stresses). Moreover, the EL of the ES processed alloy was 27.4 % (engineering strain). These results indicate simultaneous improvement of strength and ductility by ES when compared to the EX4 process. A comparison of the YS and EL reported in the literature and in this work is presented in Fig. 5b [29–36]. Although the YS of some Mg-RE alloys is higher than 300 MPa, the corresponding EL is usually low. The GW103 alloy fabricated by the ES process in this work had an excellent combination of strength and ductility. The reasons accounting for this improvement will be examined in the discussion part.

3.3. Texture characteristics

XRD measurements were carried out to measure the crystallographic texture of the GW103 alloy deformed by the two processes. The results are shown in Fig. 6 in forms of $\{10\bar{1}0\}$ and {0002} pole figures, and also by IPF, constructed for the ED direction. An usual extrusion texture of Mg was observed after extrusion [33], see in Fig. 6a: a nearly continuous fiber where the < 0002 > directions (i.e. the c axis of the hexagonal cell) were perpendicular to the ED. The maximum intensity of the fiber is not exactly at $< 10\bar{1}0 >$ || ED. A slight deviation can be seen in the IPF of the ED direction in Fig. 6a. The texture obtained by EBSD showed more clearly that the maximum region was actually at $< 20\bar{2}1 >$ || ED (see in Discussion Section), similar to the results in Refs. [37,38] for pure Mg. Thus, by adding high volume fraction of RE, the texture did not change much with respect to pure Mg [37,38], at least with a relatively small extrusion ratio of 4.

The recently reported texture component with c-axis parallel to the ED [39] and called the "RE texture components" with $< 2\bar{1}\bar{1}1 >$ - $< 2\bar{1}\bar{1}4 >$ || ED in Mg-RE alloy with heavy RE element content [6, 40–42] were not clearly detected in the present textures. Only the $< 2\bar{1}\bar{1}3 >$ appeared distinctly in the inverse pole figure of Fig. 6a, in the EX4 sample, with a very low intensity.

Fig. 6b shows the texture evolution of the ES processed sample. As the ES process was finishing with ECAP deformation, the ideal shear texture components of Mg were traced in the $\{10\bar{1}0\}$ and {0002} pole figures, and identified by their names in Fig. 6c. They are called as the B, P, Y, C1, and C2 fibers [43,44]. The locations of the ideal orientations are presented in the ideal shear plane - shear direction reference system in Fig. 6b-c. One can clearly identify in Fig. 6b the presence of the B and C2 fibers, and the P1 orientation

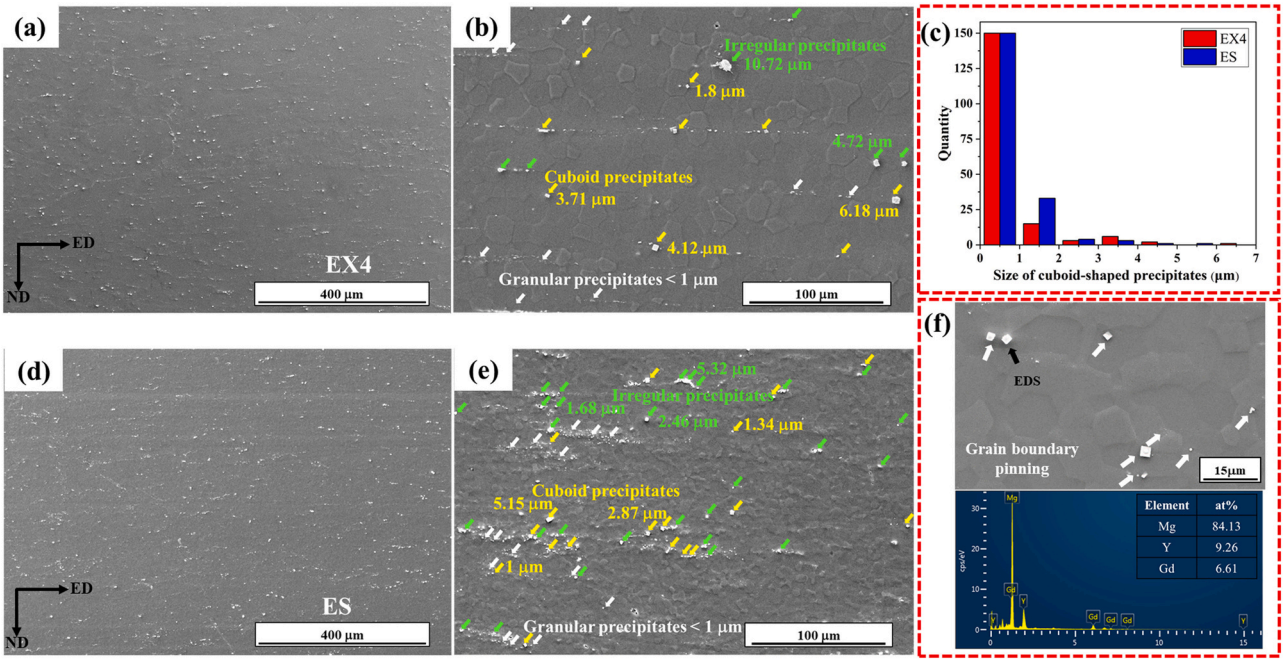

Fig. 3. Precipitate evolution in the EX4 (a, b) and ES processed (d, e) samples. (c) The size - statistics of cuboid shaped precipitates in (3b) and (3e), and (f) EDS analysis on the ES sample.

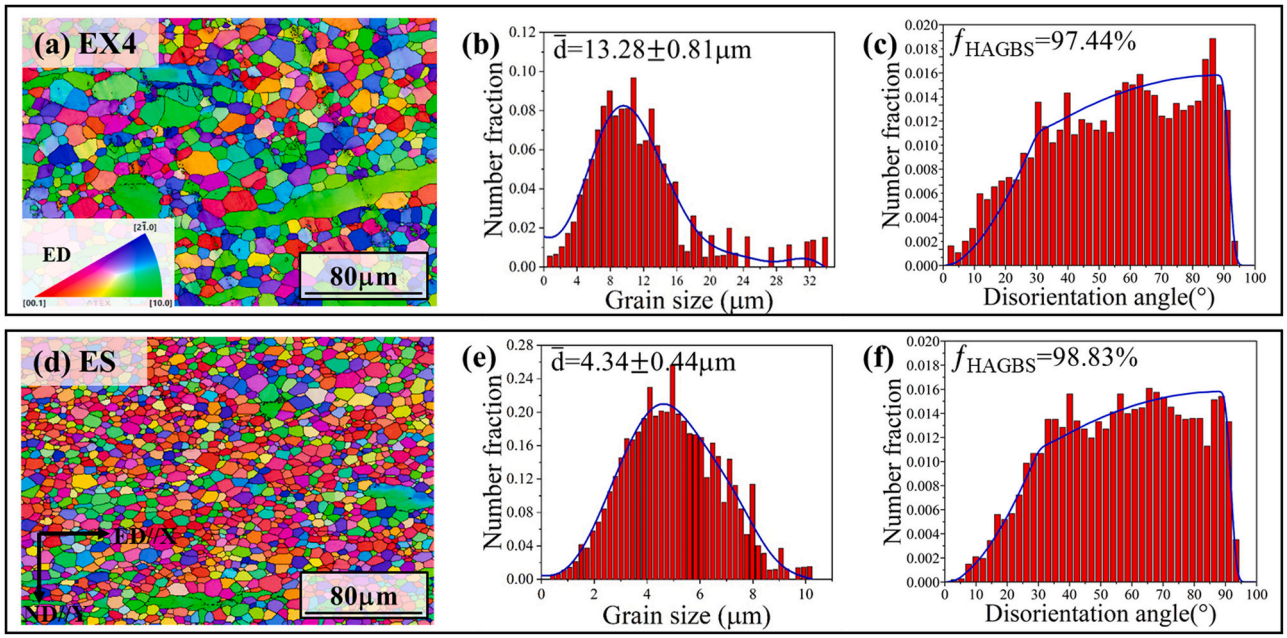

Fig. 4. EBSD IPF maps for the ED direction of (a) EX4, and (d) ES processed samples. The corresponding grain size distributions are shown in (b), (e), together with the disorientation angle distributions in (c), (f), respectively.

which is part of the P fiber. There are some components that do not belong clearly to the ECAP-shear texture, they are probably shear-rotated components of the preceding EX4 extrusion process.

In order to evaluate the strengths of the textures, the scalar texture index J is also presented in Fig. 6. J can be computed from the ODF,* it is defined by:

$$J = \int_g f(g)^2 dg, \tag{4}$$

where $f(g)$ is the is the ODF intensity at the orientation g. The texture was strong after the EX4 process (J =9.8), and weakened substantially during the subsequent C-ECAP process to J = 5.3.

4. Discussion

The new processing technique proposed in the present work led to a material which had high strength and high ductility at the same time. These mechanical properties are determined by the

* In many publications, the maximum ODF intensity is used to represent the strength, and called as 'texture intensity'. That 'intensity', however, is just a single local value of the f(g) function, so cannot represent properly the overall texture strength.

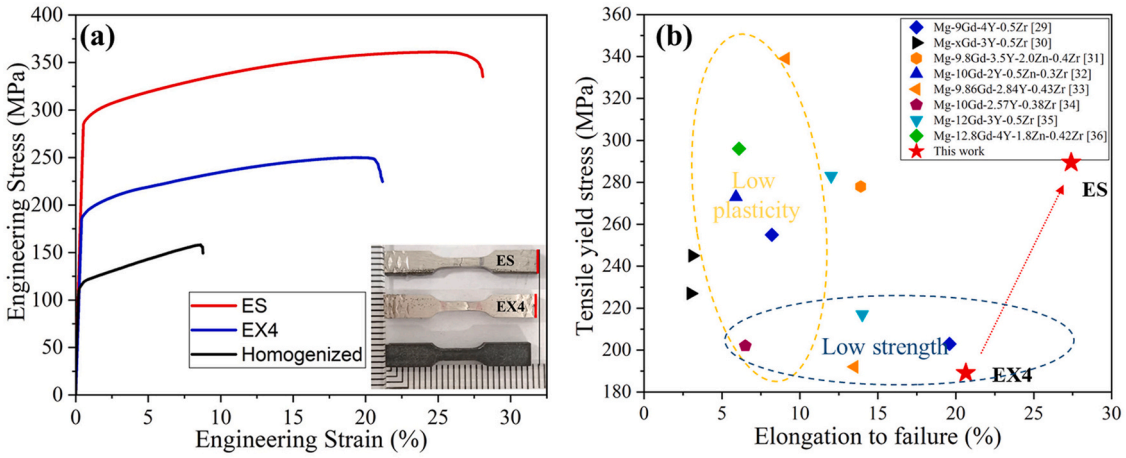

Fig. 5. (a) Engineering Stress-Engineering Strain curves obtained in tensile testing at room temperature of the initial homogenized, EX4 and ES processed samples. (b) Tensile properties of typical wrought Mg-Gd-Y alloys under room temperature.

Table 2
Tensile properties of samples obtained after different processing.

Processing states	Tensile properties		
	YS (MPa)	UTS (MPa)	EL (%)
Homogenized	117.8 ± 2.3	158.0 ± 2.6	8.33 ± 1.4
EX4	189.1 ± 6.2	249.9 ± 4.8	20.64 ± 3.3
ES	289.4 ± 4.2	361.1 ± 8.1	27.40 ± 3.5

microstructure and the crystallographic texture. The high imposed strain together with the elevated processing temperature (400 °C for a Mg alloy) led to changes in grain size and produced a new texture, which were beneficial for strength and ductility. Therefore, one has to examine the grain fragmentation process to understand the new exceptional properties. The strength was increased via the Hall-Petch relation, the possible dynamic recrystallization processes, which increase ductility, and also modify the texture. First, we examine the dynamic recrystallization because it can affect the texture evolution. Then, the texture evolution will be discussed. Finally, the mechanical properties will be explained.

4.1. Dynamic recrystallization

The occurrence of DRX can be analyzed with the help of the orientation maps obtained by EBSD. It is now an effective method to use the value of the Kernel average disorientation angle ($\Delta\theta$). It can be calculated from the orientation distributions of the pixels that form a grain in EBSD. When the value of $\Delta\theta$ is less than 2°, the grain can be considered as a grain that underwent DRX. For angles $\Delta\theta > 2°$, the grain is highly distorted by dislocations, so it is considered as a "deformed" grain. Fig. 7 displays these two categories of grains in three kinds of maps for the two deformation processes. For each case, the first map shows the DRX grains in blue color, the deformed grains in red. The fraction of DRX grains for EX4, and ES accounted for 76 %, and 95.5 %, respectively. Similar results were also reported in a previous investigation [13], in which a critical imposed extrusion strain determining the degree of DRX was established. For a similar RE contained Mg alloy, Yu et al. [45] proposed that the critical extrusion strain is 3.4 for the as extruded Mg-Gd-Y alloy, beyond which a fully recrystallized microstructure with fine DRX grains can be obtained. In the present study, the applied extrusion strains were maximum 2.54 and 3.69 for EX4 and ES, respectively. So, for EX4, where the strain was smaller than the critical one, a bimodal microstructure consisting of fine DRX grains and coarse deformed grains were obtained. On the contrary, in the ES process the microstructure was not bimodal, and a much smaller grain size (4.3 μm) was obtained. This result reveals the excellent grain fragmentation capacity of the ES process. The reason for the better performance of the ES process can be looked for in two changes. One is the strain path change that took place during the process after the first extrusion part, changing from axisymmetric deformation into shear. The other is the better effectiveness of the grain fragmentation process in shear deformation. Such an effect has been observed experimentally by comparing rolling and shear in terms of grain refinement. It was found in Cu that the grain size in ECAP is smaller than that in rolling [46]. The physical reason for this is in the lattice rotation rate, which is higher in shear than in rolling, leading to higher lattice curvature and better grain fragmentation process. The simulation using the theory for lattice rotation induced grain fragmentation introduced by Tóth et al. [47] explained this difference.

The shear deformation mode favors the recrystallization process of this Mg alloy, achieving a further grain refinement as compared to the extrusion deformation mode [48,49]. The ES processed sample exhibited more homogenous and uniform microstructure due to the addition of two shearing stages. It is probable that both DRX processes; DDRX (discontinuous DRX) and CDRX (continuous DRX), were operated in the present alloy. Nevertheless, discontinuous dynamic recrystallization (DDRX) is the main grain refinement process in the temperature range of 300–450 °C [50,51], which coincides with this work. Whereas, CDRX is the main mechanism for producing grain refinement due to plastic strain, and was visibly occurring in the ES processed alloy, as seen in Fig. 7e. CDRX is detectable in EBSD images by the formation of similar colored groups of grains, as indicated in the figure. DDRX, however, does not have a distinct feature in the microstructure in EBSD. Nevertheless, it is clear that the mechanism of the generation of refined grains is a combined effect of DDRX and CDRX.

Generally, DDRX is occurring at second phase particles, at GBs, triple junctions and deformation bands in Mg alloy [52,53]. In this study, the distribution of DRX regions and second phase particles was coincident. Particle pinning is another effect in DRX by small precipitates located at or near the GBs or triple junctions, which

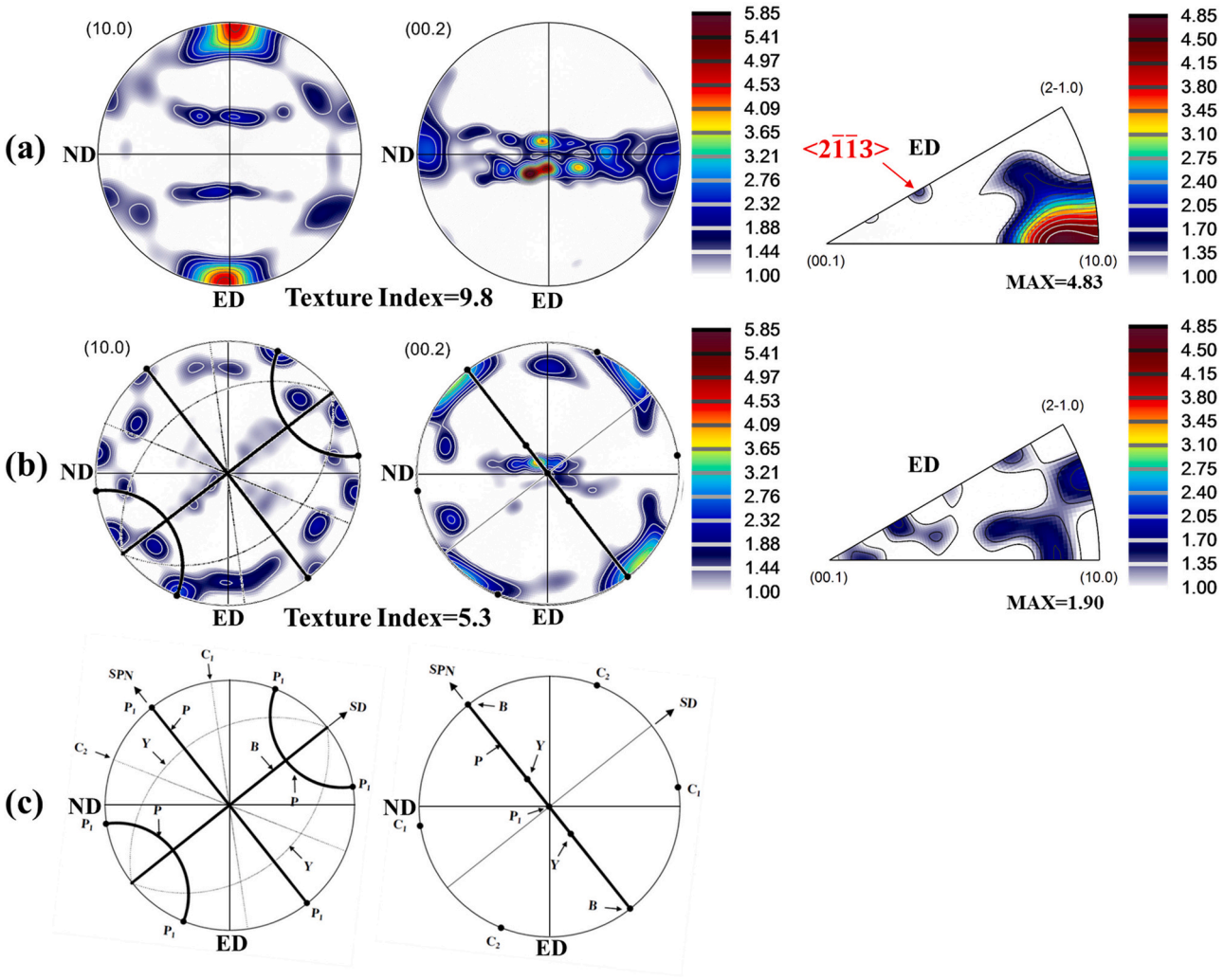

Fig. 6. Textures measured after deformation by (a) EX4, and (b) ES processes of the GW103 alloy. The textures are presented in {10$\bar{1}$0}, {0002} pole figures, and in IPF of the ED projection. (c) is the ideal shear texture positions of Mg for the present ES test (adopted from [44]).

impede the mobility of GBs. It is generally recognized that, for Mg alloy containing a second phase, small particles could pin boundaries and dislocations to retard recrystallization as shown in Fig. 3f, whereas particles larger than 1 μm can act as nucleation sites and promote the recrystallization behavior by the PSN (particle stimulated nucleation) effect [54,55]. This could be the reason for the high DRX fraction in the ES process.

The DRX process is strongly related to the crystallographic texture as well, because DRX is taking place during plastic deformation, so the intensities of the different texture components can produce preferences for the orientations of the DRX grains. More information can be obtained by examining the inverse pole figures of EBSD maps, where the two categories of grains; DRX and deformed grains, can be separated. Fig. 8 shows the result of such analysis, where the same criteria were used for classifying the grains as for the maps in Fig. 7.

The ED inverse pole figure for the EX4 deformed sample shows clearly that the main texture component was the < 20$\bar{2}$1 > || ED (Fig. 8a). The grains that belonged to this main component were mostly deformed grains (Fig. 8c), while DRX grains were mostly oriented in the < 2$\bar{1}\bar{1}$0 > || ED direction. The same texture component was observed in extruded AZ31 alloy and it was considered to form via CDRX [52]. Finally, only the deformed grains have a distinct orientation preference in the ES process: the < 10$\bar{1}$0 > || ED. All other DRX orientations in ES have the same preference as the general texture intensity. This analysis proves again, that the ES process is distinguished by its highest DRX fraction, which was 95.5 %. The reasons for the orientation frequencies of the DRX grains probably can be related to their plastic strain energy. Such correspondence has been shown for several cases, the first analysis was in the work of Refs. [56,57], however, it was in copper. For confirming similar relation for the present hexagonal alloy, polycrystal ductility simulations are needed, which will be developed in a future work.

4.2. Texture evolution

As can be seen in Fig. 6, the end-textures obtained during the two deformation processes were very different. In order to understand the textures, one has to consider all deformation components that are acting during the process. The main deformation in extrusion is a lengthening of the sample with contraction in the diameter. However, there are also redundant shear strain components, which are not negligible for the used geometries of the dies. There are two places where these shears are acting; they are illustrated in Fig. 1b. Between the two locations, the sign of the shear is inverted. This situation is very similar to the ECAP phase of the ES process, however, the main difference is that in ES-ECAP there is only shear, while in EX4, the major deformation mode is the extrusion strain, not the

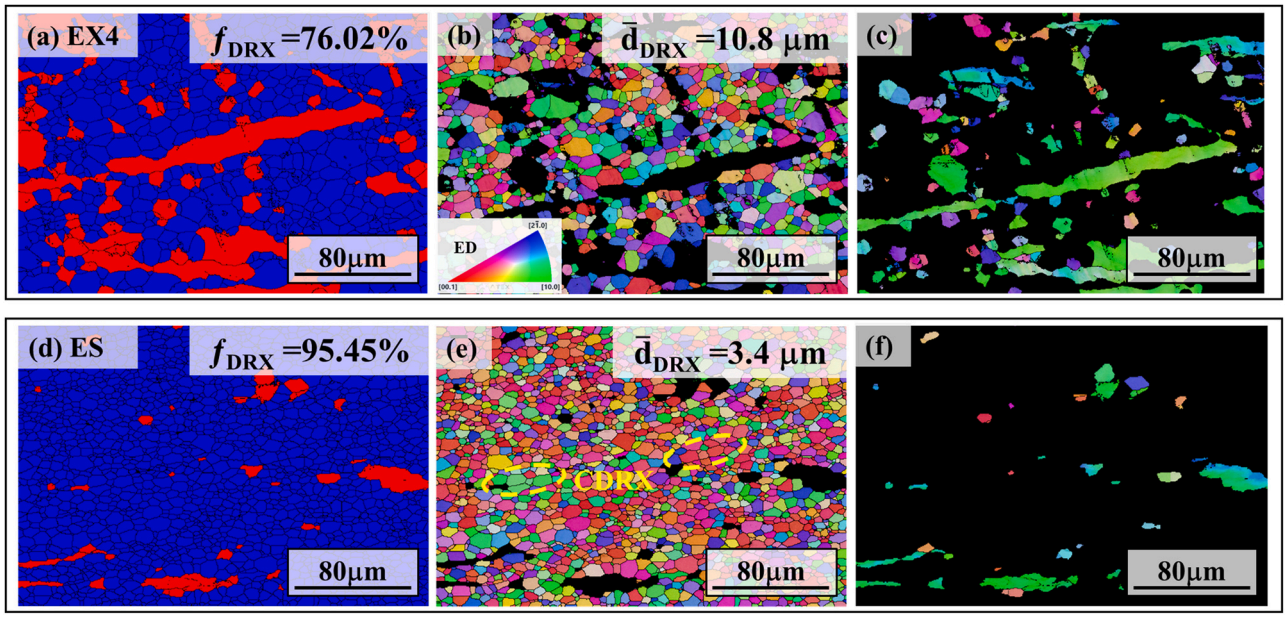

Fig. 7. Recrystallization behavior during the two deformation processes using the Kernel average disorientation angle as a criterion. (a), (d): DRX grains are in blue, deformed grains in red. (b), (e): orientation maps for the DRX grains, black color indicates deformed grains. (c), (f): orientation map of deformed grains, DRX grains are black.(For interpretation of the references to colour in this figure legend, the reader is referred to the web version of this article.)

shear. The amount of the equivalent strain corresponding to the redundant shear from the geometry is given in Table 1.

The consequence of the redundant shear in the extrusion processes is the formation of the so-called cyclic-texture, mostly known in drawing deformation [58–60]. Due to the shear process, the axial symmetry of the texture is lost, so the normally expected continuous fiber textures are not complete. This can be seen in the texture after the EX4 process in Fig. 6a.

The contribution of redundant shear to the material properties is positive. This shear, with its varying direction (always pointing towards the center of the bar), is randomizing the texture, permitting in this way a more isotropic deformation.

Only a small RE texture component was in the EX4 texture, as presented in the results section above. The presence of the RE texture components can be expected after the EX4 process, however, the extrusion ratio of only 4 seems to be low to form such components. Indeed, the RE texture components were only detected when the extrusion ration was at least 20 and/or at higher temperature (about 450 °C or above). Such a texture component is attributed to the effect of activation of non-basal slip with increasing the RE elements solution in Mg [42]. It is very probable that the redundant shear strains play a role in the formation of the RE texture components (see indicated in Fig. 1b), and will be further investigated in our future works.

The texture obtained during the ES process led to a characteristic ECAP shear texture (Fig. 6b), with some components that were originating from the first part of the ES process, the EX4. Another main change that happened in the texture of the ES process, right after the EX4 was completed, was a decrease in the strength of the texture to almost half of the strength of EX4. This texture change is helping to

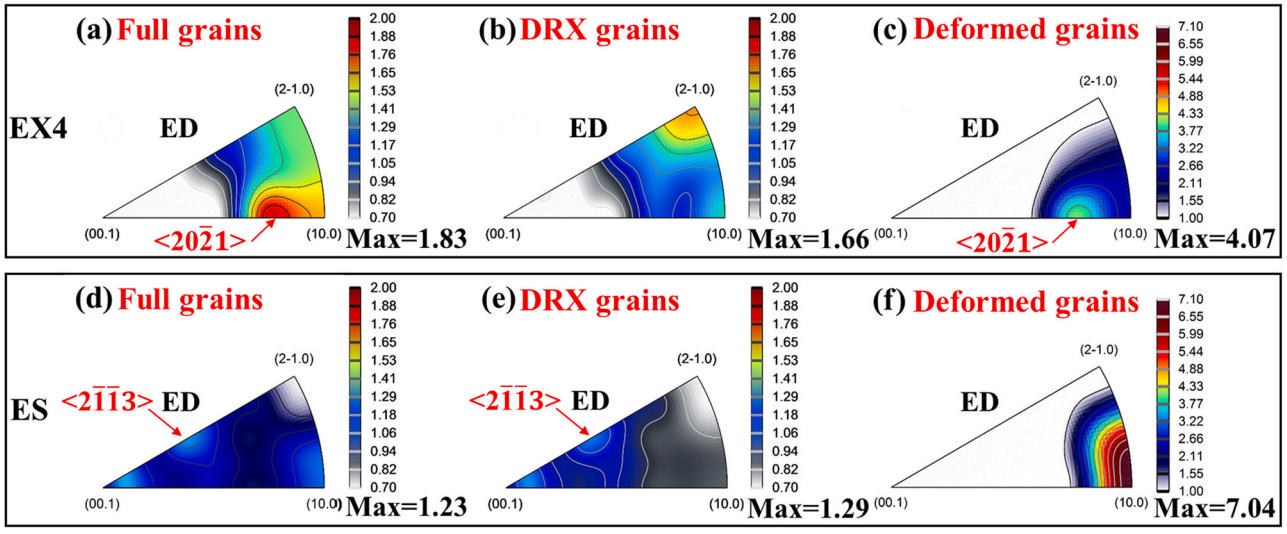

Fig. 8. Inverse pole figures of (a), (d), full grains; (b), (e), DRX and (c), (f), deformed grains, observed by EBSD, after the EX4 and ES processes.

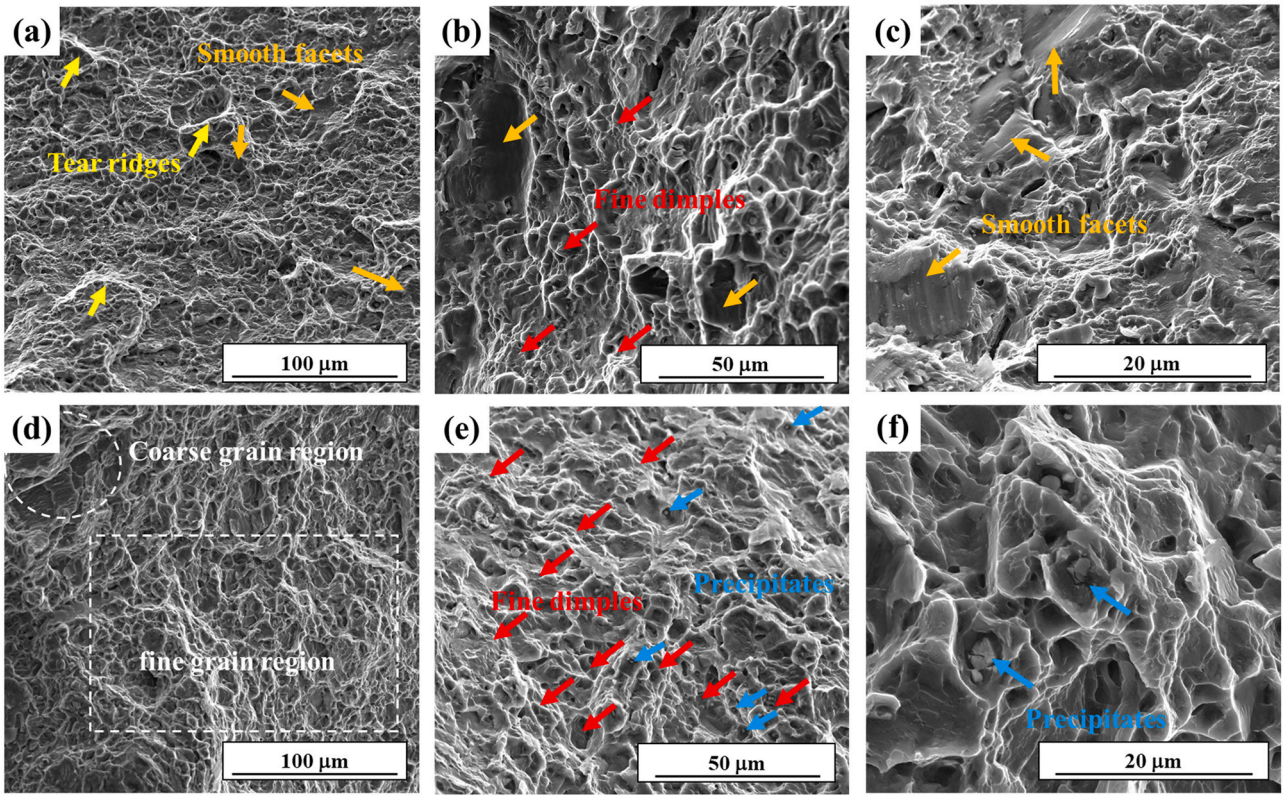

Fig. 9. SEM based fracture morphology at different magnifications of the EX4 (a, b, c) and ES-deformed (d, e, f) sample after tensile test at room temperature.

have more ductility of the material because adjacent grains have higher orientation differences, so can accommodate strain differences more easily by activating different slip systems.

This study is an example for the strong relation between texture and formability characteristics, which is especially enhanced for hcp materials. After the EX4 process, the texture is a fiber texture with basal planes parallel to the loading axis in tensile testing (Fig. 6a). For such orientations, the easiest slip system, which is basal slip for Mg alloys, cannot be activated in the subsequent tensile testing. The prismatic systems are in favorable position; however, they are harder than the basal systems. This texture effect represents a major contribution to the increased strength of the material in tensile testing. At the same time, there are only three prismatic slip systems, which is too few for a tensile testing, so the ductility of the material is limited. However, as Fig. 6 demonstrates very well, this relatively hard fiber texture is totally replaced by another one in the ES process, which consists mainly of shear texture components. Therefore, the easiest basal systems become available for slip, together with other slip systems, and good ductility can be achieved. Strength is also high, for another reason: because the grain size is very small after the ES process.

4.3. Strength and ductility

In this work, EX followed by shear in the ES process have been adopted to achieve the combination of grain refinement and texture modification, contributing to an excellent strength-ductility balance. Based on the detailed microstructure characterization in the present study, the high strength of the GW103 alloy is attributed to the mixed strengthening mechanism from grain boundary strengthening (grain refinement after ES process, σ_{GB}), solute solution strengthening (σ_{ss}), precipitation hardening (σ_{PPt}), disperse strengthening (Mg_5RE phase) and texture strengthening. By applying the methods as reported in Refs. [61–63], an estimation for the values for σ_{GB}, σ_{ss} and σ_{PPt} were 162.2–205.6 MPa, 105.8 MPa and 1.56 MPa, respectively. To sum up, the final YS obtained by ES process should be in the range of 270–313 MPa, which confirms the result of the tensile test. After the EX4 extrusion process, a traditional strong "basal" texture component with $< 10\bar{1}0 >$ || ED was formed, which was based on the dominated basal slip, leading to a weak ductility of the Mg alloy [40]. The basal-type of texture formed during the first extrusion stage was radically changed into a multi-component texture, which improved ductility. Basal-texture weakening has been proved to be a good method for improving the ductility of Mg alloys under tension test at RT [64,65].

With further refinement of the grain structure during the C-ECAP stage, the ES process led to a grain size as small as 4.3 μm. When grain size is smaller than 10 μm, grain boundary sliding (GBS) is reported to be active in deformation of Mg alloys, which induces a reduction or randomization in texture evolution and a great contribution to ductility [66–69]. Therefore, at the average grain size of 4.3 μm, GBS was probably a deformation mechanism during the tensile testing of our alloy.

Additionally, the simultaneous improvement in strength and ductility between the initial homogenized state through the EX4 and ES processes can be interpreted by the combined effects of reduced twinning and enhanced grain fragmentation, as follows. The strength and ductility measurements were done at room temperature, by tensile testing. As the present initial homogenized alloy displays twinning at RT, its ductility is limited. However, as the EX4 process was at 400 °C, there was no twinning during EX4, so it could be well deformed, and the grain size decreased due to plastic deformation. After EX4, during the tensile testing at RT, twinning was reduced because twinning in hexagonal materials is grain size dependent: by reducing the grain size, the twinning activity is decreasing. Therefore, because of the smaller grain size, the strength increased, while ductility also increased, because twinning was reduced. In the ES testing, there was further plastic deformation at

400 °C, so there was more grain refinement. Therefore, the RT tensile test showed even higher strength. Ductility has also increased, because twinning was totally suppressed, due to the even smaller grain size.

The SEM morphologies of the fracture surface under tension at room temperature are shown in Fig. 9 for the EX4 and ES sample. Some tear ridges and smooth facets appear on the EX4 fracture surface, which are commonly considered as brittle fracture features in Mg alloys [70]. On the contrary, one can see large number of fine dimples (red arrows) in the ES sample, indicating ductile fracture. Meanwhile, precipitates (blue arrows) were also observed at the bottom of the dimples which were evidencing the improvement for strength.

5. Conclusions

In the present work, the extrusion-shearing process (ES) was applied to refine the microstructure of the Mg-10Gd-3Y alloy for the purpose of simultaneously improving strength and ductility, compared to the conventional extrusion (EX). The tensile yield strength of the alloy was increased to 289 MPa with a high ultimate tensile strength of 361 MPa, and a good tensile elongation to failure EL of 27.4% was obtained. Microstructural characterizations showed that the additional shearing deformation by the second stage of the ES process (the C-ECAP) facilitated the formation of a fully recrystallized homogenous microstructure with an average grain size of about 4.3 µm with dynamic precipitations of $Mg_5(Gd,Y)$ particles at/near grain boundaries. The observation of fracture morphology revealed ductile feature for the ES-processed sample. The multi-component texture and microstructural modification of grain refinement and dispersive distribution of precipitates all contributed to the excellent combination of high strength and ductility of the Mg-10Gd-3Y alloy processed by ES.

The main conclusion of this work is that changing the processing route during thermo-mechanical processing can be very beneficial for material properties. It has been demonstrated that traditional one-step extrusion process combined with ECAP is a very efficient technique to obtain Mg-RE alloy with high performance.

CRediT authorship contribution statement

Cai Chen: Conceptualization, Methodology, Writing – original draft, Project administration, Funding acquisition. **Dongsheng Han:** Methodology, Formal analysis, Investigation, Data curation, Visualization, Writing – review & editing. **Shun Xu:** Validation, Writing – review & editing. **Mingchuan Wang:** Resources, Funding acquisition. **Ting Cai:** Investigation, Visualization. **Sen Yang:** Validation. **Fengjian Shi:** Methodology, Resources. **Benoit Beausir:** Formal analysis, Validation. **Laszlo S Toth:** Formal analysis, Writing – review & editing.

Data Availability

Data will be made available on request.

Declaration of Competing Interest

The authors declare that they have no known competing financial interests or personal relationships that could have appeared to influence the work reported in this paper.

Acknowledgments

The authors are grateful for the financial support provided by the National Natural Science Foundation of China (Grant No. 51901101, 11802131, 51901102, 52105368). This work was also supported by the french "Investment in the future" operated by the National Research Agency (ANR) and referenced by ANR-11-LABX-0008-01 (LabEx DAMAS).

References

[1] M.T. Pérez-Prado, J. Bohlen, S. Yi, D. Letzig, T. Al-Samman, J. Robson, M. Barnett, W. Poole, C. Mendis, S. Agnew, N. Stanford, Emerging hot topics and research questions in wrought magnesium alloy development, J. Min. Met. Mater. Soc. 72 (7) (2020) 2561–2567, https://doi.org/10.1007/s11837-020-04051-5

[2] Z.Z. Jin, M. Zha, S.Q. Wang, S.C. Wang, C. Wang, H.L. Jia, H.Y. Wang, Alloying design and microstructural control strategies towards developing Mg alloys with enhanced ductility, J. Magnes. Alloy. 10 (5) (2022) 1191–1206, https://doi.org/10.1016/j.jma.2022.04.002

[3] J. Song, J. Chen, X. Xiong, X. Peng, D. Chen, F. Pan, Research advances of magnesium and magnesium alloys worldwide in 2021, J. Magnes. Alloy. 10 (4) (2022) 863–898, https://doi.org/10.1016/j.jma.2022.04.001

[4] C. Su, D. Li, A.A. Luo, T. Ying, X. Zeng, Effect of solute atoms and second phases on the thermal conductivity of Mg-RE alloys: a quantitative study, J. Alloy. Compd. 747 (2018) 431–437, https://doi.org/10.1016/j.jallcom.2018.03.070

[5] Y. Zhang, W. Rong, Y.J. Wu, L.M. Peng, J.F. Nie, N. Birbilis, A detailed HAADF-STEM study of precipitate evolution in Mg–Gd alloy, J. Alloy. Compd. 777 (2019) 531–543, https://doi.org/10.1016/j.jallcom.2018.10.193

[6] J. Luo, H. Yan, L.W. Lu, R.S. Chen, A.R. Wu, F.C. Yin, Cold rollability improvement by twinning and twin–slip synergy in an Mg–Zn–Gd alloy with rare earth texture, J. Alloy. Compd. 883 (2021) 160813, https://doi.org/10.1016/j.jallcom.2021.160813

[7] J. Zhao, H. Guo, T. Luo, C. Zhang, J. Luo, Microstructure evolution and grain refinement mechanism of fine-grained Mg-Gd-Y-Zn-Zr alloy during multi-directional forging, J. Alloy. Compd. 928 (2022) 167119, https://doi.org/10.1016/j.jallcom.2022.167199

[8] S. Liu, J. Zhang, H. Yang, X. Chen, G. Huang, A. Tang, X. Chen, B. Jiang, F. Pan, Optimization in strength-ductility of heterogeneous Mg-13Gd alloy via small extrusion ratio combined with pre-aging, Mater. Sci. Eng.: A 833 (2022) 142540, https://doi.org/10.1016/j.msea.2021.142540

[9] L. Tang, W. Liu, Z. Ding, D. Zhang, Y. Zhao, E.J. Lavernia, Y. Zhu, Alloying Mg with Gd and Y: increasing both plasticity and strength, Comput. Mater. Sci. 115 (2016) 85–91, https://doi.org/10.1016/j.commatsci.2016.01.003

[10] G. Hu, B. Xing, F. Huang, M. Zhong, D. Zhang, Effect of Y addition on the microstructures and mechanical properties of as-aged Mg-6Zn-1Mn-4Sn (wt%) alloy, J. Alloy. Compd. 689 (2016) 326–332, https://doi.org/10.1016/j.jallcom.2016.06.216

[11] J. Zhang, S. Liu, R. Wu, L. Hou, M. Zhang, Recent developments in high-strength Mg-RE-based alloys: focusing on Mg-Gd and Mg-Y systems, J. Magnes. Alloy. 6 (3) (2018) 277–291, https://doi.org/10.1016/j.jma.2018.08.001

[12] J. Zheng, Z. Chen, Z. Yan, Z. Zhang, Q. Wang, Y. Xue, Preparation of ultra-high strength Mg-Gd-Y-Zn-Zr alloy by pre-ageing treatment prior to extrusion, J. Alloy. Compd. 894 (2022) 162490, https://doi.org/10.1016/j.jallcom.2021.162490

[13] C. Xu, T. Nakata, X.G. Qiao, H.S. Jiang, W.T. Sun, Y.C. Chi, M.Y. Zheng, S. Kamado, Effect of extrusion parameters on microstructure and mechanical properties of Mg-7.5Gd-2.5Y-3.5Zn-0.9Ca-0.4Zr (wt%) alloy, Mater. Sci. Eng.: A 685 (2017) 159–167, https://doi.org/10.1016/j.msea.2016.12.121

[14] T.S. Zhou, Q.F. Zhang, Q.Q. Li, L.D. Wang, Q.L. Li, D.X. Liu, A simultaneous enhancement of both strength and ductility by a novel differential-thermal ECAP process in Mg-Sn-Zn-Zr alloy, J. Alloy. Compd. 889 (2022) 161653, https://doi.org/10.1016/j.jallcom.2021.161653

[15] J. Sun, Z. Yang, J. Han, T. Yuan, D. Song, Y. Wu, Y. Yuan, X. Zhuo, H. Liu, A. Ma, Enhanced quasi-isotropic ductility in bi-textured AZ91 Mg alloy processed by up-scaled RD-ECAP processing, J. Alloy. Compd. 780 (2019) 443–451, https://doi.org/10.1016/j.jallcom.2018.12.008

[16] X. Ding, R. Chen, J. Zhang, W. Cao, Y. Su, J. Guo, Recent progress on enhancing the hydrogen storage properties of Mg-based materials via fabricating nanostructures: a critical review, J. Alloy. Compd. 897 (2022) 163137, https://doi.org/10.1016/j.jallcom.2021.163137

[17] C. Sun, H. Liu, C. Wang, J. Ju, G. Wang, J. Jiang, A. Ma, J. Bai, F. Xue, Y. Xin, Anisotropy investigation of an ECAP-processed Mg-Al-Ca-Mn alloy with synergistically enhanced mechanical properties and corrosion resistance, J. Alloy. Compd. 911 (2022) 165046, https://doi.org/10.1016/j.jallcom.2022.165046

[18] H.T. Jeong, W.J. Kim, Critical review of superplastic magnesium alloys with emphasis on tensile elongation behavior and deformation mechanisms, J. Magnes. Alloy. 10 (5) (2022) 1133–1153, https://doi.org/10.1016/j.jma.2022.02.009

[19] P. Minárik, M. Zemková, J. Veselý, J. Bohlen, M. Knapek, R. Král, The effect of Zr on dynamic recrystallization during ECAP processing of Mg-Y-RE alloys, Mater. Charact. 174 (2021) 111033, https://doi.org/10.1016/j.matchar.2021.111033

[20] H.J. Hu, Z. Sun, Z.W. Ou, X.Q. Wang, Researches on a novel severe plastic deformation method combining direct extrusion and shearings for AZ61 magnesium alloy based on numerical simulation and experiments, Met. Mater. Int. 23 (3) (2017) 582–590, https://doi.org/10.1007/s12540-017-6578-z

[21] Z. Horita, K. Matsubara, K. Makii, T.G. Langdon, A two-step processing route for achieving a superplastic forming capability in dilute magnesium alloys, Scr. Mater. 47 (4) (2002) 255–260, https://doi.org/10.1016/S1359-6462(02)00135-5

[22] A. Vinogradov, D. Orlov, Y. Estrin, Improvement of fatigue strength of a Mg–Zn–Zr alloy by integrated extrusion and equal-channel angular pressing, Scr. Mater. 67 (2) (2012) 209–212, https://doi.org/10.1016/j.scriptamat.2012.04.021
[23] H.J. Hu, Y. Liu, D.F. Zhang, Z.W. Ou, The influences of extrusion-shear process on microstructures evolution and mechanical properties of AZ31 magnesium alloy, J. Alloy. Compd. 695 (2017) 1088–1095, https://doi.org/10.1016/j.jallcom.2016.10.234
[24] J. Dong, W.C. Liu, X. Song, P. Zhang, W.J. Ding, A.M. Korsunsky, Influence of heat treatment on fatigue behaviour of high-strength Mg–10Gd–3Y alloy, Mater. Sci. Eng.: A 527 (2010) 6053–6063, https://doi.org/10.1016/j.msea.2010.06.030 (21-22).
[25] R.G. Li, H.R. Li, H.C. Pan, D.S. Xie, J.H. Zhang, D.Q. Fang, Y.Q. Dai, D.Y. Zhao, H. Zhang, Achieving exceptionally high strength in binary Mg-13Gd alloy by strong texture and substantial precipitates, Scr. Mater. 193 (2021) 142–146, https://doi.org/10.1016/j.scriptamat.2020.10.052
[26] S.M. He, X.Q. Zeng, L.M. Peng, X. Gao, J.F. Nie, W.J. Ding, Microstructure and strengthening mechanism of high strength Mg–10Gd–2Y–0.5Zr alloy, J. Alloy. Compd. 427 (1–2) (2007) 316–323, https://doi.org/10.1016/j.jallcom.2006.03.015
[27] X. Gao, S.M. He, X.Q. Zeng, L.M. Peng, W.J. Ding, J.F. Nie, Microstructure evolution in a Mg–15Gd–0.5Zr (wt%) alloy during isothermal aging at 250°C, Mater. Sci. Eng.: A 431 (1–2) (2006) 322–327, https://doi.org/10.1016/j.msea.2006.06.018
[28] B. Beausir, J.-J. Fundenberger, 2017. Analysis tools for electron and X-ray diffraction, ATEX-software, www.atex-software.eu, Université de Lorraine - Metz, 2017.
[29] Z. Xiao, X. Yang, Y. Yang, Z. Zhang, D. Zhang, Y. Li, T. Sakai, Microstructural development under interrupted hot deformation and the mechanical properties of a cast Mg–Gd–Y–Zr alloy, Mater. Sci. Eng.: A 652 (2016) 377–383, https://doi.org/10.1016/j.msea.2015.11.034
[30] H.R.J. Nodooshan, W. Liu, G. Wu, Y. Rao, C. Zhou, S. He, W. Ding, R. Mahmudi, Effect of Gd content on microstructure and mechanical properties of Mg–Gd–Y–Zr alloys under peak-aged condition, Mater. Sci. Eng.: A 615 (2014) 79–86, https://doi.org/10.1016/j.msea.2014.07.056
[31] M. Li, Y. Huang, Y. Liu, X. Wang, Z. Wang, Effects of heat treatment before extrusion on dynamic recrystallization behavior, texture and mechanical properties of as-extruded Mg-Gd-Y-Zn-Zr alloy, Mater. Sci. Eng.: A 832 (2022) 142479, https://doi.org/10.1016/j.msea.2021.142479
[32] X.Z. Han, W.C. Xu, D.B. Shan, Effect of precipitates on microstructures and properties of forged Mg–10Gd–2Y–0.5Zn–0.3Zr alloy during ageing process, J. Alloy. Compd. 509 (35) (2011) 8625–8631, https://doi.org/10.1016/j.jallcom.2011.06.086
[33] W.C. Liu, J. Dong, X. Song, J.P. Belnoue, F. Hofmann, W.J. Ding, A.M. Korsunsky, Effect of microstructures and texture development on tensile properties of Mg–10Gd–3Y alloy, Mater. Sci. Eng.: A 528 (6) (2011) 2250–2258, https://doi.org/10.1016/j.msea.2010.12.009
[34] J.L. Li, D. Wu, R.S. Chen, E.H. Han, Effects of Gd/Y ratio on the microstructures and mechanical properties of cast Mg–Gd–Y–Zr alloys, Magnes. Technol. 2019 (2019) 51–56, https://doi.org/10.1007/978-3-030-05789-3_9
[35] R. Zhu, Y. Wu, J. Liu, J. Wang, Microstructure and properties of Mg-12Gd-3Y-0.5Zr alloys processed by ECAP and extrusion, J. Wuhan. Univ. Technol. -Mater. Sci. Ed. 26 (6) (2011) 1128–1132, https://doi.org/10.1007/s11595-011-0375-1
[36] Z. Yan, Z. Zhang, X. Li, J. Xu, Q. Wang, G. Zhang, J. Zheng, H. Fan, K. Xu, J. Zhu, Y. Xue, A novel severe plastic deformation method and its effect on microstructure, texture and mechanical properties of Mg-Gd-Y-Zn-Zr alloy, J. Alloy. Compd. 822 (2020) 153698, https://doi.org/10.1016/j.jallcom.2020.153698
[37] J. Bohlen, S. Yi, D. Letzig, K.U. Kainer, Effect of rare earth elements on the microstructure and texture development in magnesium–manganese alloys during extrusion, Mater. Sci. Eng.: A 527 (26) (2010) 7092–7098, https://doi.org/10.1016/j.msea.2010.07.081
[38] N. Stanford, Micro-alloying Mg with Y, Ce, Gd and La for texture modification—a comparative study, Mater. Sci. Eng.: A (2010) 2669–2677, https://doi.org/10.1016/j.msea.2009.12.036 527(10-11).
[39] J. Wang, M.R.G. Ferdowsi, S.R. Kada, S. Babaniaris, B. Hutchinson, P.A. Lynch, M.R. Barnett, Appearance of textures with a c-axis parallel to the extrusion direction in Mg alloys, Scr. Mater. 210 (2022) 114422, https://doi.org/10.1016/j.scriptamat.2021.114422
[40] A. Imandoust, C.D. Barrett, T. Al-Samman, K.A. Inal, H. El Kadiri, A review on the effect of rare-earth elements on texture evolution during processing of magnesium alloys, J. Mater. Sci. 52 (1) (2016) 1–29, https://doi.org/10.1007/s10853-016-0371-0
[41] Z. Yang, C. Xu, T. Nakata, S. Kamado, Effect of extrusion ratio and temperature on microstructures and tensile properties of extruded Mg-Gd-Y-Mn-Sc alloy, Mater. Sci. Eng.: A 800 (2021) 140330, https://doi.org/10.1016/j.msea.2020.140330
[42] Y.J. Ma, C.M. Liu, S.N. Jiang, Y.C. Wan, Z.Y. Chen, Microstructure, mechanical properties and damping capacity of as-extruded Mg-1.5Gd alloys containing rare-earth textures, Mater. Charact. 189 (2022) 111969, https://doi.org/10.1016/j.matchar.2022.111969
[43] B. Beausir, L.S. Tóth, K.W. Neale, Ideal orientations and persistence characteristics of hexagonal close packed crystals in simple shear, Acta Mater. 55 (8) (2007) 2695–2705, https://doi.org/10.1016/j.actamat.2006.12.021
[44] B. Beausir, S. Suwas, L.S. Tóth, K.W. Neale, J.-J. Fundenberger, Analysis of texture evolution in magnesium during equal channel angular extrusion, Acta Mater. 56 (2) (2008) 200–214, https://doi.org/10.1016/j.actamat.2007.09.032
[45] Z. Yu, Y. Huang, W. Gan, Z. Zhong, N. Hort, J. Meng, 2017. Effects of extrusion ratio and annealing treatment on the mechanical properties and microstructure of a Mg–11Gd–4.5Y–1Nd–1.5Zn–0.5Zr (wt%) alloy, Journal of Materials Science 52(11) (2017) 6670–6686, doi.org/10.1007/s10853–017-0902–3.
[46] C.F. Gu, L.S. Tóth, M. Arzaghi, C.H.J. Davies, Effect of strain path on grain refinement in severely plastically deformed copper, Scr. Mater. 64 (3) (2011) 284–287, https://doi.org/10.1016/j.scriptamat.2010.10.002
[47] L.S. Tóth, Y. Estrin, R. Lapovok, C. Gu, A model of grain fragmentation based on lattice curvature, Acta Mater. 58 (5) (2010) 1782–1794, https://doi.org/10.1016/j.actamat.2009.11.020
[48] H. Chen, B. Song, N. Guo, T. Liu, T. Zhou, J. He, Dynamic recrystallization and grain refinement in extruded AZ31 rod during hot torsion deformation at 150 °C, Met. Mater. Int. 25 (1) (2018) 147–158, https://doi.org/10.1007/s12540-018-0177-5
[49] P. Minárik, R. Král, J. Pešička, S. Daniš, M. Janeček, Microstructure characterization of LAE442 magnesium alloy processed by extrusion and ECAP, Mater. Charact. 112 (2016) 1–10, https://doi.org/10.1016/j.matchar.2015.12.002
[50] A. Galiyev, R. Kaibyshev, G. Gottstein, Correlation of plastic deformation and dynamic recrystallization in magnesium alloy ZK60, Acta Mater. 49 (7) (2001) 1199–1207, https://doi.org/10.1016/S1359-6454(01)00020-9
[51] S. Biswas, B. Beausir, L.S. Toth, S. Suwas, Evolution of texture and microstructure during hot torsion of a magnesium alloy, Acta Mater. 61 (14) (2013) 5263–5277, https://doi.org/10.1016/j.actamat.2013.05.018
[52] M.G. Jiang, C. Xu, H. Yan, G.H. Fan, T. Nakata, C.S. Lao, R.S. Chen, S. Kamado, E.H. Han, B.H. Lu, Unveiling the formation of basal texture variations based on twinning and dynamic recrystallization in AZ31 magnesium alloy during extrusion, Acta Mater. 157 (2018) 53–71, https://doi.org/10.1016/j.actamat.2018.07.014
[53] J.P. Hadorn, K. Hantzsche, S. Yi, J. Bohlen, D. Letzig, J.A. Wollmershauser, S.R. Agnew, Role of solute in the texture modification during hot deformation of Mg-rare earth alloys, Metall. Mater. Trans. A 43 (4) (2011) 1347–1362, https://doi.org/10.1007/s11661-011-0923-5
[54] T. Al-Samman, Modification of texture and microstructure of magnesium alloy extrusions by particle-stimulated recrystallization, Mater. Sci. Eng.: A 560 (2013) 561–566, https://doi.org/10.1016/j.msea.2012.09.102
[55] J.D. Robson, D.T. Henry, B. Davis, Particle effects on recrystallization in magnesium–manganese alloys: Particle-stimulated nucleation, Acta Mater. 57 (9) (2009) 2739–2747, https://doi.org/10.1016/j.actamat.2009.02.032
[56] J.J. Jonas, L.S. Tóth, Modelling oriented nucleation and selective growth during dynamic recrystallization, Scr. Metall. Et. Mater. 27 (11) (1992) 1575–1580, https://doi.org/10.1016/0956-716X(92)90147-7
[57] L.S. Tóth, J.J. Jonas, Modelling the texture changes produced by dynamic recrystallization, Scr. Metall. Et. Mater. 27 (3) (1992) 359–363, https://doi.org/10.1016/0956-716X(92)90526-K
[58] A. Abdellaoui, T. Montesin, J.J. Heizmann, J.B. Pelletier, Study of the texture of steelcord during the wet drawing process-influence of the patenting and the friction on the dies, Mater. Sci. Forum 157- 162 (1994) 611–616, https://doi.org/10.4028/www.scientific.net/MSF.157-162.611
[59] S. Li, S. He, A. Van Bael, P. van Houtte, FEM-Aided taylor simulations of radial texture gradient in wire drawing, Mater. Sci. Forum (2002) 439–444, https://doi.org/10.4028/www.scientific.net/MSF.408-412.439 408-412.
[60] C.F. Gu, L.S. Tóth, R. Lapovok, C.H.J. Davies, Texture evolution and grain refinement of ultrafine-grained copper during micro-extrusion, Philos. Mag. 91 (2) (2010) 263–280, https://doi.org/10.1080/14786435.2010.518987
[61] X. Li, W. Qi, K. Zheng, N. Zhou, Enhanced strength and ductility of Mg–Gd–Y–Zr alloys by secondary extrusion, J. Magnes. Alloy. 1 (1) (2013) 54–63, https://doi.org/10.1016/j.jma.2013.02.006
[62] H. Yu, C. Li, Y. Xin, A. Chapuis, X. Huang, Q. Liu, The mechanism for the high dependence of the Hall-Petch slope for twinning/slip on texture in Mg alloys, Acta Mater. 128 (2017) 313–326, https://doi.org/10.1016/j.actamat.2017.02.044
[63] H. Cai, F. Guo, J. Su, L. Liu, B. Chen, Study on microstructure and strengthening mechanism of AZ91-Y magnesium alloy, Mater. Res. Express 5 (3) (2018), https://doi.org/10.1088/2053-1591/aab0b7
[64] C.F. Gu, L.S. Tóth, D.P. Field, J.J. Fundenberger, Y.D. Zhang, Room temperature equal-channel angular pressing of a magnesium alloy, Acta Mater. 61 (8) (2013) 3027–3036, https://doi.org/10.1016/j.actamat.2013.01.063
[65] P.C. Gautam, S. Biswas, On the possibility to reduce ECAP deformation temperature in magnesium: deformation behaviour, dynamic recrystallization and mechanical properties, Mater. Sci. Eng.: A 812 (2021) 141103, https://doi.org/10.1016/j.msea.2021.141103
[66] S. Hémery, C. Tromas, P. Villechaise, Slip-stimulated grain boundary sliding in Ti-6Al-4 V at room temperature, Materialia 5 (2019) 100189, https://doi.org/10.1016/j.mtla.2018.100189
[67] A. Varma, A. Gokhale, H. Krishnaswamy, D.K. Banerjee, J. Jain, Grain boundary sliding and non-constancy strain during stress relaxation of pure Mg, Mater. Sci. Eng.: A 817 (2021) 141349, https://doi.org/10.1016/j.msea.2021.141349
[68] L.S. Toth, C. Gu, Ultrafine-grain metals by severe plastic deformation, Mater. Charact. 92 (2014) 1–14, https://doi.org/10.1016/j.matchar.2014.02.003
[69] W. Mohamed, S. Gollapudi, I. Charit, K.L. Murty, Formability of a wrought Mg alloy evaluated by impression testing, Mater. Sci. Eng.: A 712 (2018) 140–145, https://doi.org/10.1016/j.msea.2017.11.088
[70] J.X. Wei, H. Yan, R.S. Chen, Notch strength and notch fracture mechanisms of a cast Mg-Gd-Y alloy, Mater. Sci. Eng.: A 835 (2022) 142668, https://doi.org/10.1016/j.msea.2022.142668